The United Nations University

GEOTHERMAL TRAINING PROGRAMME
Orkustofnun, Grensásvegur 9,
IS-108 Reykjavík, Iceland

Reports 1996
Number 10

ANALYSIS OF INJECTION AND TRACER TESTS DATA FROM THE OLKARIA-EAST GEOTHERMAL FIELD, KENYA

Cornel Otieno Ofwona
Kenya Power & Lighting Company Ltd.
Olkaria Geothermal Project,
P.O. Box 785, Naivasha,
KENYA

ABSTRACT

Reinjection is the planned strategy for dealing with the decline in steam production, falling reservoir pressures and the disposition of waste geothermal water in the Olkaria-East geothermal field. This report presents a simple one-dimensional (1-D) fracture model analysis of data obtained during the 1993 injection and tracer test experiment in which well OW-03 was the injection well. The model estimates a cross-sectional area of 210 m^2 to connect wells OW-03 and OW-04. Based on this fracture area, cooling calculations show that injection rates of less than 50 m^3/hr would be preferable and that hot water injection (>100 °C) would be better than cold.

1. INTRODUCTION

The Olkaria geothermal field is situated in the eastern branch of the great Rift Valley and located about 125 km north west of Nairobi, the capital city of Kenya (Figure 1). The field is divided into four sectors namely East, Northeast, West and Central.

Active geothermal exploration work in Olkaria started in 1970. In 1973, the first deep exploration well was drilled to a depth of 1003 m. A second exploration well drilled about 3.5 km to the north of the first well led to the discovery of a two-phase reservoir. Using the information from this well (OW-02), other off-set wells, OW-03, OW-04 and OW-05, were drilled within 250 m distance of it (Odongo, 1993).

Subsequent investigation of the area led to the commissioning of the first 15 MW_e power plant in 1981 and two others in 1982 and 1985 giving a total current capacity of 45 MW_e. Thirty three wells have been drilled in this field (Olkaria-East) seven of which are make-up wells for steam decline in wells producing since 1981. A total of 30 wells have been drilled in Olkaria-NE field and discharge tests of these wells have proven a steam equivalent of 74 MW_e and already a design for the construction of a 2 x 32 MW_e plant is being planned. The Olkaria-West and the Olkaria-Central sectors are still under exploration.

Reinjection is the planned strategy in Olkaria-East field for managing the decline in steam production and falling reservoir pressures as well as the disposal of polluting waste water. This strategy is based

on an injection and tracer test experiment which was conducted between April and September 1993 in which OW-03 was used as the injection well. The experiment showed that reinjection was feasible and an increase in production was observed from OW-04 (Ambusso, 1994).

The objective of this report is to use the data from this test and do an analysis to establish the geometrical properties of the subsurface flow channels which connect the injection and production wells. Based on these geometrical properties, the long term thermal efficiency of injection in this part of the field will be studied, with my understanding of the subject as taught during the 1996 Geothermal Training Programme of the United Nations University, Iceland.

2. AN OVERVIEW OF THE OLKARIA-EAST GEOTHERMAL FIELD

2.1 Geological structure

Figure 1 shows the main geological structures of the Olkaria geothermal field. The field is associated with the Olkaria volcanic centre and the reservoir is considered to be bounded by arcuate faults forming a ring or a caldera structure (Naylor, 1972). The heat source for the geothermal fluids in the area is consequently related to this volcano. N-S and E-W trending faults and fractures are prominent in the area with other inferred faults striking almost NW-SE.

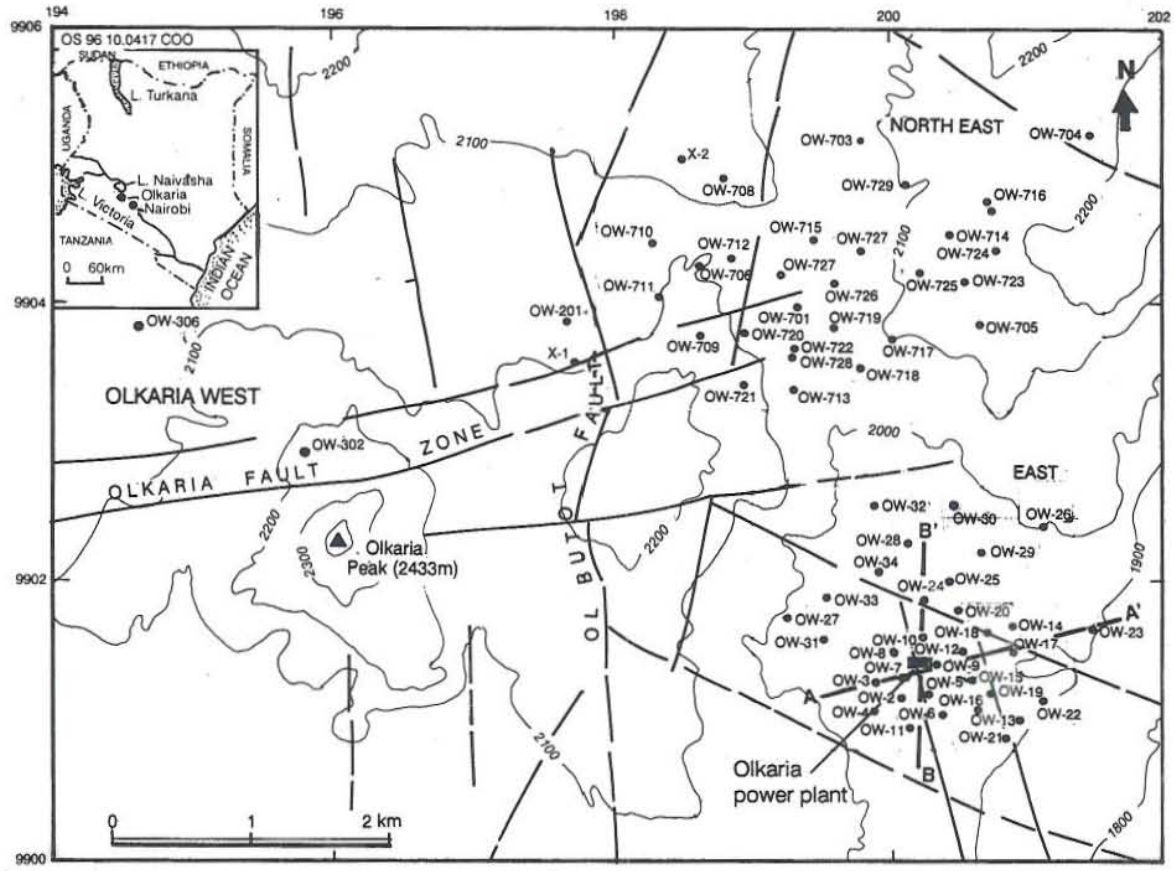

FIGURE 1: Location of wells and geological structures in the Olkaria geothermal field, Kenya

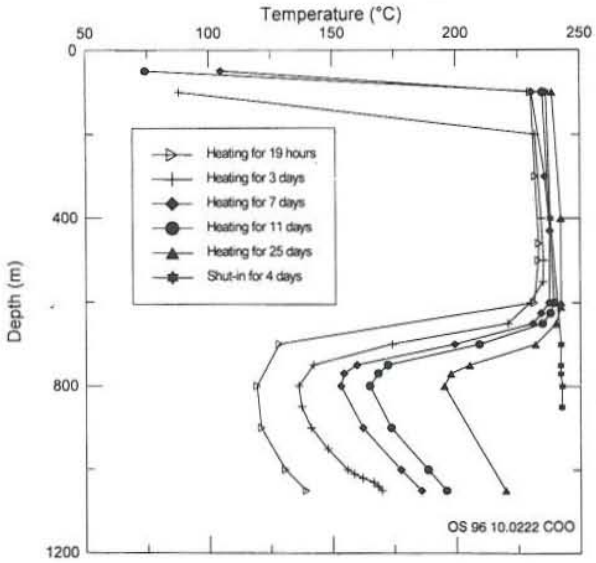

FIGURE 2: Temperature profiles in well OW-14

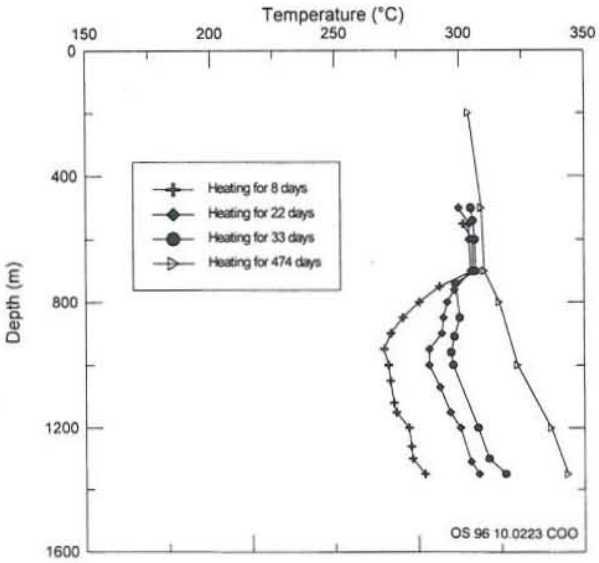

FIGURE 3: Temperature profiles in well OW-21

2.2 Temperature and pressure distribution

Figures 2-5 show temperature and pressure profiles for wells OW-14, OW-21 and OW-04 taken during heating up periods. From the temperature profiles, it is observed that there exists a region of very rapid recovery at 400-700 m depth. Temperatures in this region are close to 240°C. A comparison of the temperature and pressure profiles shows that this fast recovery is due to boiling in the wells where they encounter the reservoir's steam zone. Deeper into the wells, there is a region of temperature inversion. This inversion is temporary and eventually disappears as seen in Figures 3 and 5. It is caused by cooling during the drilling operation and its recovery is slower than the upper steam region. The equilibrium temperature and pressure profiles follow the boiling point depth curve in this interval.

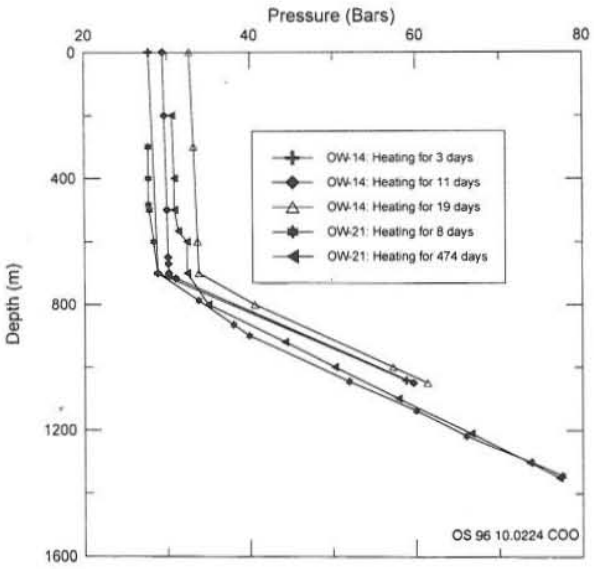

FIGURE 4: Pressure profiles in wells OW-14 and OW-21

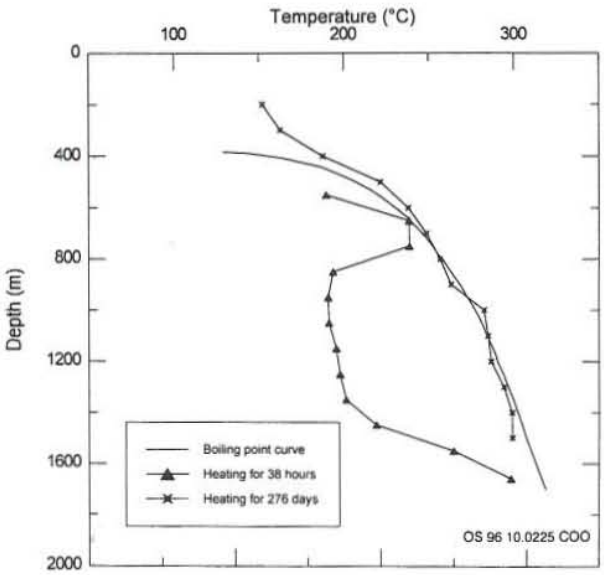

FIGURE 5: Temperature profiles in well OW-04

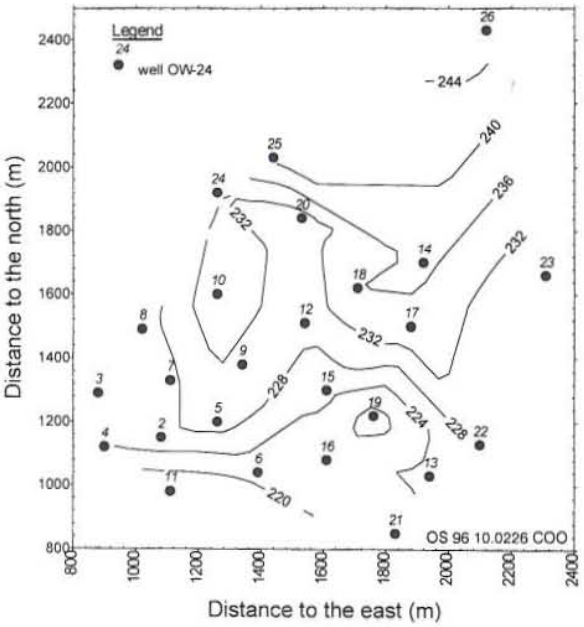

FIGURE 6: Formation temperature distribution in °C at 1250 m a.s.l.

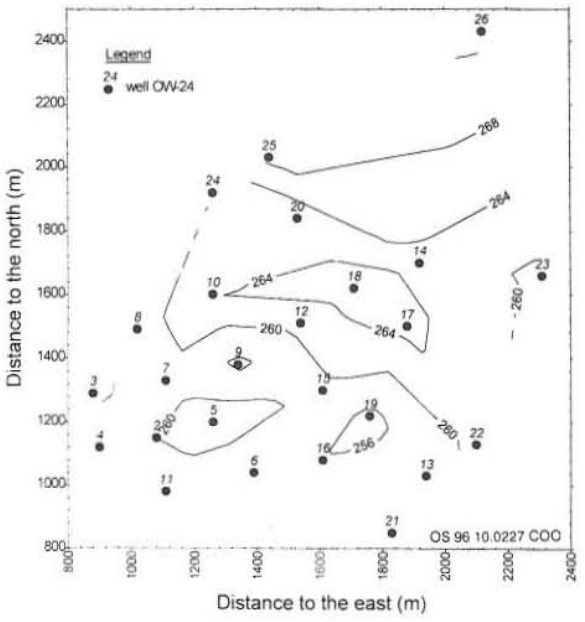

FIGURE 7: Formation temperature distribution in °C at 1000 m a.s.l.

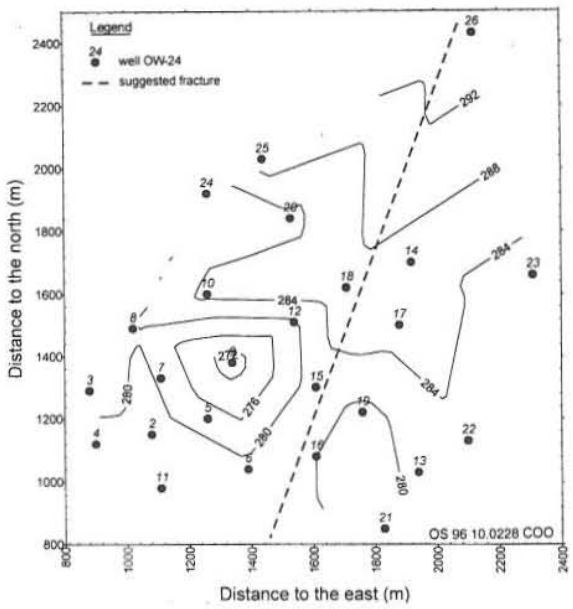

FIGURE 8: Formation temperature distribution in °C at 750 m a.s.l.

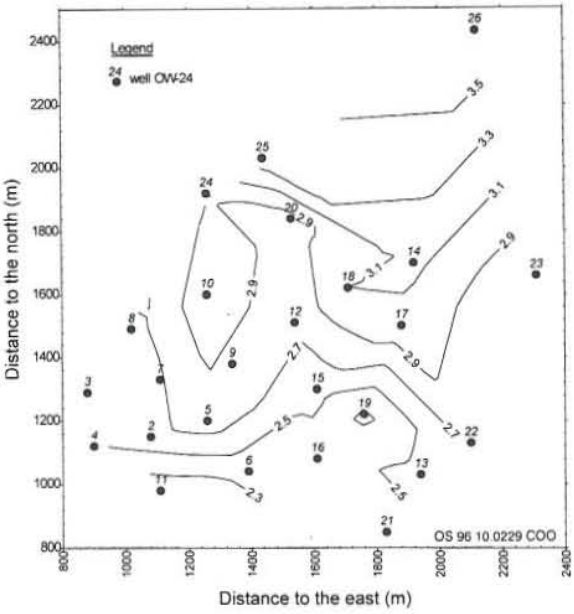

FIGURE 9: Initial pressure distribution in MPa at 1250 m a.s.l.

Planar views of formation temperature and initial pressure distributions at different elevations are shown in Figures 6-10. Observation of the planar temperature and pressure distribution shows in general a decline in temperatures and pressures from north to south indicating a north-south flow of the reservoir fluid. The possible existence of a fracture across the well field (Figure 8) is addressed in section 3.2.

2.3 Fluid chemistry

Table 1 shows results obtained from geochemical analysis of water samples from some wells in the Olkaria-East field (Merz and McLellan-Virkir, 1986). The water discharged from deep wells is relatively dilute and of sodium-chloride type. Some, but not large, variations occur in the composition of water discharged from individual wells. The deeper and hotter aquifers are higher in dissolved solids. This is explained by boiling and steam loss at greater depths within the reservoir and condensation of the ascending steam at higher levels.

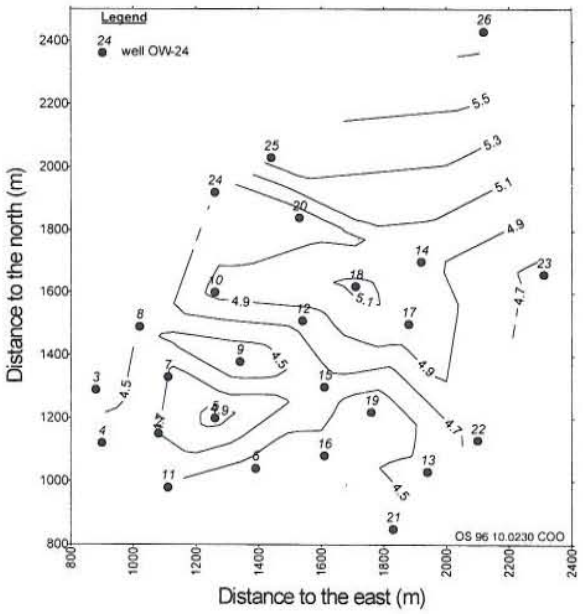

FIGURE 10: Initial pressure distribution in MPa at 1000 m a.s.l.

2.4 Regional hydrology

The water recharge to the geothermal reservoir is assumed to originate from the Lake Naivasha catchment area in the north (see Figure 1). This water percolates down through deep vertical fissures which run N-S across the field. The fissures allow the water access to the deep heat source where lateral flow and heat transfer may take place. Infiltration from other directions is also possible (Merz and McLellan-Virkir, 1981).

TABLE 1: Chemical composition of water in ppm discharged from wells in Olkaria-East

Well No.	pH	SiO_2	Na	K	B	Ca	Mg	CO_2	SO_4	H_2S	Cl	F	TDS
OW-02	8.40	813	625	100	10	-	-	32	18	2	935	78	2498
OW-03	9.10	650	540	78	5	-	-	62	28	3	630	70	2054
OW-04	9.00	600	470	60	10	-	-	69	38	2	653	79	1888
OW-05	9.00	605	400	60	4	-	-	59	31	3	440	81	1622
OW-06	9.10	675	500	75	6	-	-	40	29	4	610	54	-
OW-07	8.50	775	730	135	9	-	-	73	23	2	1039	35	2860
OW-08	9.10	525	400	44	5	-	-	53	41	-	380	-	-
OW-09	9.00	610	460	51	6	-	-	132	52	-	430	-	-
OW-10	9.10	713	475	93	6	-	-	25	29	3	720	62	-
OW-11	9.10	594	450	78	5	-	-	60	25	2	640	71	2010
OW-12	8.90	613	420	55	8	-	-	89	42	5	545	70	1876
OW-13	9.70	705	415	55	4	-	-	25	34	19	350	94	1850
OW-14	9.55	700	535	60	10	-	-	14	57	9	520	110	2034
OW-15	8.50	795	530	105	10	-	-	19	43	2	880	52	2460
OW-16	8.40	746	414	65	8	-	-	27	64	2	620	80	2100
OW-17	8.80	595	414	80	10	-	-	27	67	4	550	79	1820
OW-18	8.50	607	650	110	14	.1	.1	15.3	19	-	920	62	2680
OW-19	8.50	541	920	180	20	-	.1	30.5	40	4.42	1508	37	3679
OW-20	9.10	760	522	100	10	-	-	-	31	-	740	43	-
OW-21	9.20	597	390	59	5	3	.2	148	76.6	2.04	459	32	-
OW-22	9.60	631	407	56	1	.4	.1	16.4	10	14.4	228	155	-
OW-23	9.40	229	200	54	2	-	-	126	37	8	257	175	1516
OW-24	9.30	241	310	64	2	-	-	72.9	42.3	6.2	408	60	1616
OW-25	9.00	267	381	66	3	-	.1	63.2	55	3.7	443	74	1698
OW-26	9.10	239	195	29	1	-	-	15	29	3.1	164	72	1148

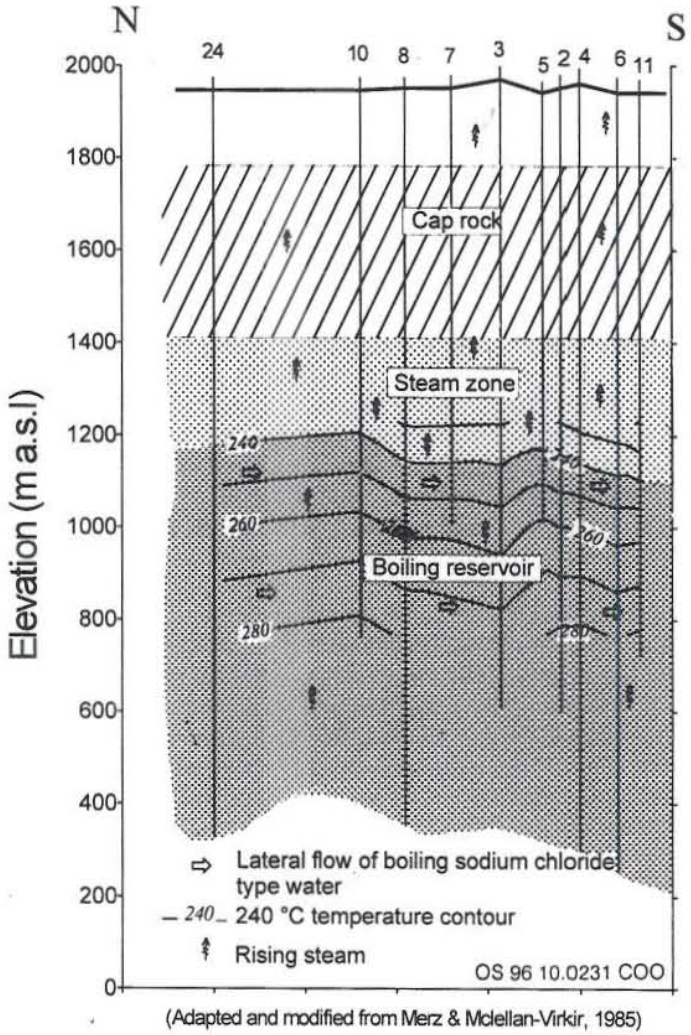

FIGURE 11: A pre-exploitation conceptual reservoir model for the Olkaria-East geothermal field

2.5 Conceptual reservoir model

Figure 11 presents a pre-exploitation conceptual reservoir model for the Olkaria-East geothermal field (Merz and McLellan-Virkir, 1985). Above 1400 m a.s.l., the wells penetrate a basaltic lava cap rock which shields a steam zone trapped between 1150-1400 m a.s.l. This steam zone can easily be identified from the near isothermal sections in the downhole temperature profiles and the vapour static pressure gradient in the pressure profiles (Figures 2-5). Below the steam zone, there is a boiling liquid dominated reservoir with a steam/water interface temperature of 240°C. Chemical geothermometers have predicted deep reservoir temperatures in excess of 300°C. The highest measured temperature in this field is 341°C at -540 m a.s.l. in well OW-19 (KPC, 1984).

There is a lateral flow of boiling reservoir fluid from north to south caused by a pressure gradient resulting from the upflow zone existing to the north of this field (KPC, 1984). As the fluid boils, it produces steam which rises up, convecting heat to the surrounding rocks.

3. WELL CHARACTERISTICS

3.1 General information

A typical well casing programme for Olkaria wells consists of 20" diameter surface casing, 13 3/8" diameter anchor casing, 9 5/8" diameter production casing and 7" diameter slotted liners (Figure 12). Total drilled depths and status of wells in the East Production Field are shown in Table 2 below. Data from the seven make up wells (OW-27 to OW-34) were not available for this study.

3.2 Lithology and aquifers

Table 3 summarizes the results of well completion and discharge tests for Olkaria-East wells. The transmissivity values were obtained from fall-off and recovery tests. They range from 0.06-5.7 Dm. Permeable horizons in the wells occur at 900-1200 m a.s.l., 600-800 m a.s.l. and 300-500 m a.s.l. Feed zones at 900-1200 m a.s.l. are richer in steam than the deeper ones. Most wells in this field are cyclic due to alternate production from the steam and liquid dominated feed zones.

Discharge enthalpies obtained during flow tests ranged from 1800-2672 kJ/kg but have been increasing with time due to expansion of the steam zone during exploitation. Total mass flow rates obtained from early discharge tests ranged from 11.7-68.2 tons/hr (3.25-19 kg/s) and have also been declining with time due to exploitation. It is worth noting at this point that the best producers in this field are wells OW-26 (47 t/hr), OW-18 (35.4 t/hr), OW-15 (30.5 t/hr) and OW-16 (68.2 t/hr). All these wells seem to be located on the same line as shown in Figure 8 and observation of the temperature contours suggests a fluid movement from the north along this line. Based on these observations, one can conclude that there could be a N-S fracture in this locality.

Stratigraphic cross-sections for the wells in Olkaria-East are shown in Figures 13 and 14 (see Figure 1 for location). The reservoir rocks consist of successive strata of rhyolite, trachyte, and basalt. Producing horizons occur mostly at contacts between lavas but fractures in the rocks are also important (Merz & McLellan, 1981).

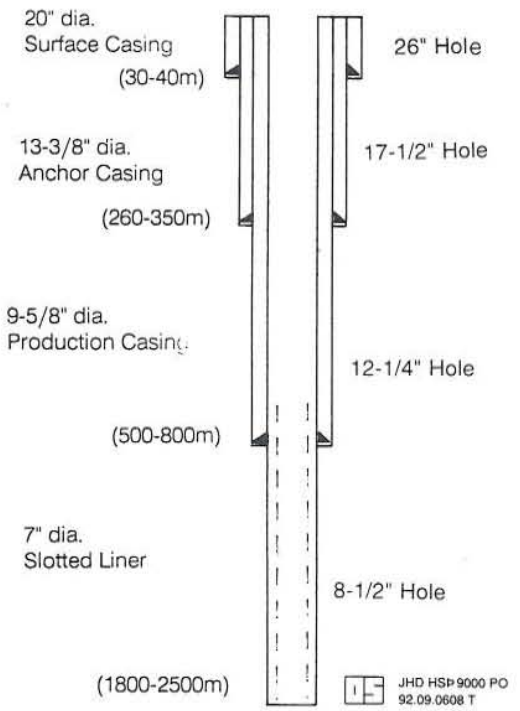

FIGURE 12: A typical casing programme for Olkaria wells

TABLE 2: An overview of Olkaria-East wells

Well No.	Elevation (m a.s.l.)	Eastings (m)	Northings (m)	Depth (m)	Production casing (m)	Status of well
OW-01	2068.4			1003	418.0	Unproductive
OW-02	1941.0	200080	9901150	1350	594.5	Productive
OW-03	1957.8	199880	9901290	1357	682.0	Unprodcutive
OW-04	1949.9	199900	9901120	1661	698.0	Productive
OW-05	1928.8	200260	9901200	910	660.7	"
OW-06	1930.1	200390	9901040	1685	630.0	"
OW-07	1938.9	200110	9901330	1308	627.0	"
OW-08	1941.3	200020	9901490	1600	541.6	"
OW-09	1927.5	200340	9901380	1181	548.1	Plugged
OW-10	1933.3	200260	9901600	1183	547.8	Productive
OW-11	1932.3	200110	9900980	1221	514.7	Productive
OW-12	1928.8	200540	9901510	901	497.2	"
OW-13	1921.1	200940	9901030	1049	537.5	"
OW-14	1948.4	200920	9901700	1069	488.7	"
OW-15	1925.9	200610	9901300	1301	519.8	"
OW-16	1929.3	200610	9901080	1304	636.3	"
OW-17	1936.1	200880	9901500	1234	544.5	"
OW-18	1941.6	200710	9901620	1407	539.6	"
OW-19	1931.9	200760	9901220	2485	948.9	"
OW-20	1935.0	200530	9901840	1406	545.4	"
OW-21	1921.5	200830	9900850	1394	537.2	"
OW-22	1923.9	201100	9901130	1404	547.0	"
OW-23	1940.0	201310	9901660	1292	527.5	"
OW-24	1935.3	200260	9901920	1618	558.4	"
OW-25	1941.6	200440	9902030	1604	546.5	
OW-26	2006.5	201120	9902430			

TABLE 3: Characteristics of Olkaria-East wells (Merz & McLellan-Virkir, 1986)

Well No.	Feed zones (m) L: Liquid dominated S: Steam dominated	Transmissivity (x 10^{-8} m^3/Pa s)		Flowing enthalpy (kJ/kg)	Av. total flow (tons/hr)
		Fall-off test	Recovery test		
OW-02	700-750 (S); 900 (L), 1100 (L)			2150	25.2
OW-03	700-800 (S); 900 (L), 1100 (L)				
OW-04	750-850 (S); 1300-1400 (L), 1450-1600 (L)			1800	32 (cyclic)
OW-05	700 (S), 800 (L)			2647	25
OW-06	850 (L)		0.85	2383	13.3
OW-07	750-800 (L)			2104	12 (cyclic)
OW-08	550-700 (S); 900-1080 (L), 1200-1400 (L)	2.8	2.3	2530	16
OW-09	600 (S), 720 (S); 1060 (L),		1.5		
OW-10	650-670 (S); 900 (L), 1100 (L)		1.9	2548	20.9
OW-11	725-750 (S); 1150-1200 (L)		1.6	1982	23.4
OW-12	575 (S), 750 (S); 850-900 (L)		2.3	2563	35.2
OW-13	600-650 (S); 850-900 (L)		5.7	2115	15.9
OW-14	600-700 (S); 900-1000 (L)		2.0	2562	12 (cyclic)
OW-15	700-800 (S); 1100-1175 (L)		1.8	2672	30.5
OW-16	700-750 (S), 1125-1150 (L)		4.1	2215	68.2
OW-17	545-600 (S); 800-900 (L), 1150 (L)	0.8	0.3	2362	12
OW-18	540-600 (S); 800-900 (L), 1150 (L)	1.7	1.3	2643	35.4
OW-19	1000-1050 (L), 1550-1600 (L)	0.4	0.06	2545	21.6
OW-20	750-850 (L), 1050-1200 (L), 1300 (L)	1.1	0.4 - 1.4	2547	25.3
OW-21	700-750 (S); 1000-1125 (L), 1275-1300 (L)	0.65	4.9	2237	19.8
OW-22	700-750 (S); 1000 (L)	1.0	4 - 13	2169	21.3
OW-23	530-700 (S); 900-1000 (L), 1250 (L)	2.1	5.5	2160	11.7
OW-24	550-700 (S); 1050-1100 (L)	4.0	2.9	2475	26.3
OW-25	550-650 (S); 1200-1400 (L)	2.1	3.3	1992	20.4
OW-26	570-625 (S); 750-800 (L), 1300 (L)	2.1		1900	47

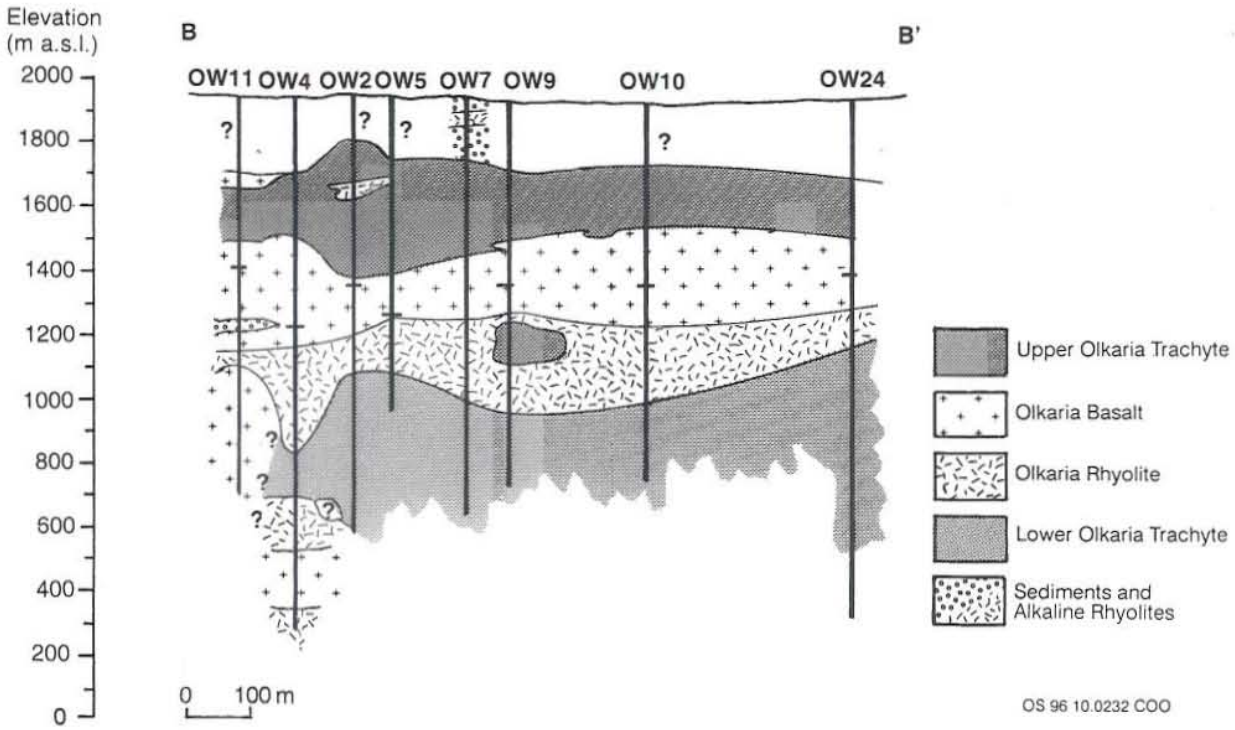

FIGURE 13: A N-S geological section of Olkaria-East wells

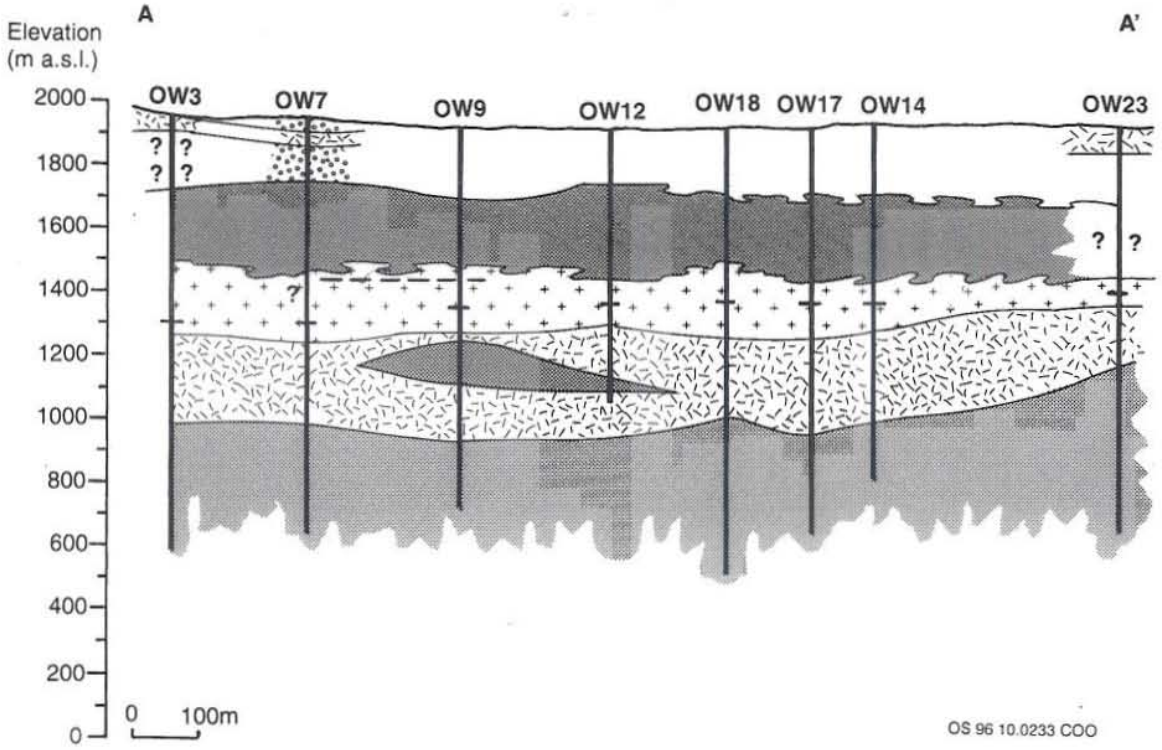

FIGURE 14: An E-W geological section of Olkaria-East wells

4. MODELING FLOW OF HEAT AND TRACERS IN A FRACTURE

4.1 The 1-D fracture approach

Modelling flow of heat in a fractured system is generally complicated and often requires a numerical approach. However, simple analytical modelling may apply for idealised circumstances. A 1-D analytical modelling approach was applied by Björnsson et al. (1994) in a feasibility study of Thelamörk, a fractured low-temperature geothermal field in Iceland. The 1-D fracture approach will also be used in the study described in this report for the following reasons:

1. Olkaria is considered to be a fractured system, therefore, we can assume that the flow channels connecting injection and production wells are predominantly fractures.
2. The 1-D model of tracer concentration applies directly to fracture flow and also to conductive heat transfer between the same fracture and the formation.
3. The tracer data is used to estimate the geometrical dimensions of the flow channel and thus provides important input parameters for the heat transfer model of the same fracture.
4. The 1-D fracture model approach takes a relatively short time compared to detailed numerical methods. It also involves relatively few input parameters making it ideal for a training study.

4.2 Tracer flow in a fracture

Consider an injection-production well dipole connected by a fracture zone (Figure 15). Fluid is produced at a constant rate, Q, from the production well and injected at a constant rate, q, to the injection well. At time $t = 0$, a mass M of some tracer is injected as a slug and consequently transported along the flow

channel to the production well. Fluid samples of the produced fluid are taken regularly at times $t > 0$ and analysed for the concentration of the tracer, $c(t)$. The cross-sectional area of the flow channel connecting the two wells is $A = h \times b$, where h is the height and b is the width. The porosity of the flow channel is ϕ and its longitudinal dispersivity is denoted by α_L.

The following basic assumptions are used in formulating the history of tracer concentration in the flow channel:

1. The flow channel connecting the two wells is along a narrow fracture zone.
2. The flow is one dimensional.
3. Molecular diffusion is neglected.
4. Injection and production rates are constant.

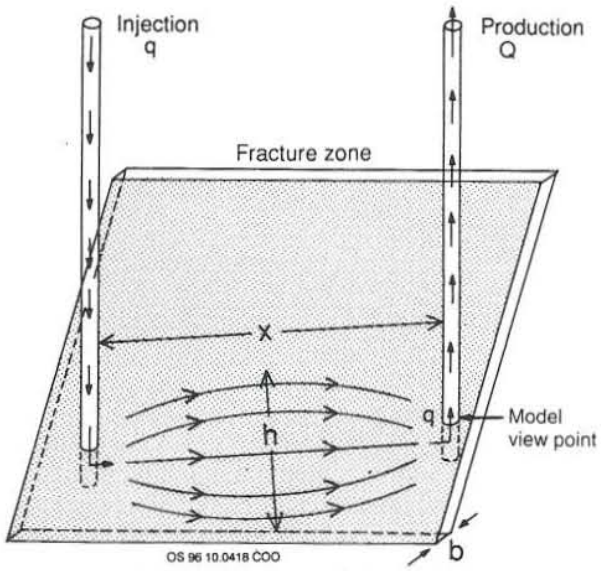

FIGURE 15: A simple model of a fracture zone connecting injection-production well dipole

The differential equation describing tracer concentration in the flow channel, C, is then represented by (Javandel et al., 1984)

$$D\frac{\partial^2 C}{\partial x^2} = u\frac{\partial C}{\partial x} + \frac{\partial C}{\partial t} \qquad (1)$$

where x is the distance from the injection well, t the time, u the mean velocity of the flow ($u = q/\rho A\phi$) and D the dispersion coefficient of the flow channel ($D = \alpha_L u$), the initial and boundary conditions being

$$C(x,0) = 0; \quad C(x,t) = 0 \quad when \quad x \to \infty$$

$$M = \int_0^\infty \phi C(x,t)\,dx$$

The tracer concentration in the produced fluid, c, is correlated to the fracture zone concentration, C, by using the conservation of mass, i.e. $cQ = Cq$. Therefore, solving the governing equation results in

$$c(t) = \frac{uM}{Q}\,\frac{1}{2\sqrt{\pi Dt}}\,\exp\frac{-(x-ut)^2}{4Dt} \qquad (2)$$

The unknown parameters in Equation 2 are u, M and D. A computer inversion program, TRINV, is available for matching this equation with the tracer recovery curve obtained in the field (Arason and Björnsson, 1994). From the values of u, M and D, one may solve for the desired cross-sectional area, $A\phi$, of the flow channel connecting the injection and production wells.

4.3 Heat flow in a fracture

The analysis of tracer return curves provides an estimate of the cross-sectional area, A, of the flow channel and hence the total contact area between the reservoir rock and the injected fluid. Given the flow channel inlet temperature, T_{inj}, the channel height, length and width as well as the initial reservoir temperature, T_0, the temperature of the injected fluid, T, at any distance x along the flow channel can be estimated by considering the heat convected along the flow channel (Equation 3) and the heat conducted perpendicularly into the fracture from the reservoir rock (Equation 4) (Bödvarsson, 1969)

$$\textit{Convective heat flow:}\quad \rho_w C_w b \frac{\partial T}{\partial t} + C_w \frac{q}{h} \frac{\partial T}{\partial x} = 2k \frac{\partial T}{\partial y} \tag{3}$$

$$\textit{Conductive heat flow:}\quad \frac{\partial^2 T}{\partial y^2} = \frac{\rho_r C_r}{k} \frac{\partial T}{\partial t} = \frac{1}{\alpha} \frac{\partial T}{\partial t} \tag{4}$$

where ρ is density, C is heat capacity, k is thermal conductivity of the rock and α its thermal diffusivity. The subscripts w and r refer to water and rock respectively.

A solution to this set of equations is given by Carlslaw and Jaeger (1959):

$$T_{out}(x,t) = T_{inj} + (T_0 - T_{inj})\ erf\ [\frac{kxh}{C_w q \sqrt{\alpha(t - x/\beta)}}] \tag{5}$$

and is valid at times $t > x/\beta$, with β defined as $q/\rho_w hb$. The temperature of the produced fluid, assuming a constant temperature, T_0, for all feed zones in the production well, except the one connected to the flow channel, is finally given by the principle of energy conservation:

$$T(t) = T_0 - \frac{q}{Q} [T_0 - T_{out}] \tag{6}$$

These two equations can be used to estimate the temperature of the injected fluid as it enters the production well either as the flow channel temperature at the sandface (Equation 5) or as the temperature of the total flow (Equation 6). Note the importance of the term β. It involves the product hb of the flow channel cross sectional area and is obtained from the analysis of the tracer recovery curve (Equation 2).

5. ANALYSIS OF INJECTION AND TRACER TEST DATA

5.1 The injection experiment

A joint injection and tracer test was done in the Olkaria-East field during April to September 1993 (Ambusso, 1994). During the test, a total of 413,542 m^3 of 18 °C fresh water from Lake Naivasha was injected into well OW-03 for 172 days giving an average injection rate of 100 m^3/hr (28 kg/s). All the production wells around OW-03 were monitored for changes in steam flow, water flow and discharge

enthalpy. After the first 45 days of injection, 125 kg of sodium-fluorescein, a chemical tracer, were introduced into the injection well over a 1¼ hour period with the water flow stopped, hence, representing a slug injection into the reservoir. The results of the test were published in a report by Ambusso (1994).

In the next sections of this report, the author performs an analysis of the injection data using the simple fracture model described in section 4.2 to find the geometrical properties of the possible flow channels connecting the injection and production wells.

5.2 Observed changes in the production wells during injection

Figure 16 shows daily measured water flow rate from well OW-02 which is located 217 m from the injection well OW-03. Due to cycling of the well, the data was filtered using a Gausian type filter and the resulting curve is also shown in Figure 16. The filtered data indicates that there was a gradual rise in water output from the start of the injection experiment to a maximum value where it remained for about 100 days before falling and rising again. Figure 17 shows that average steam flow rate from this well remained steady both during and after the injection test and that there was the gradual fall in water flow rate after the injection was stopped. This indicates that the increase in water output from well OW-02 is due to injection. The gradual rise of water output during injection and then gradual fall when the injection is stopped may indicate that the connection between OW-03 and OW-02 is not via a fracture flow but rather through a matrix flow of a long thermal time constant. Note also from Figure 16 that the breakthrough of injected water into well OW-02 made the well more cyclical in water flow than before the test.

Figure 18 shows weekly average output values from well OW-04 which is 185 m away from OW-03. When the water injection was stopped, an almost immediate drop in water flow was observed in this well. The steam flow remained rather constant but there was an increase in enthalpy. This is also an indication that the injection affected the water flow and enthalpy during the experiment. The increase in enthalpy when injection was stopped may indicate that the water which was entering well OW-04 from the injection well was "cold". The immediate response in water flow when the injection was stopped suggests that a fracture connects the OW-03 → OW-04 dipole.

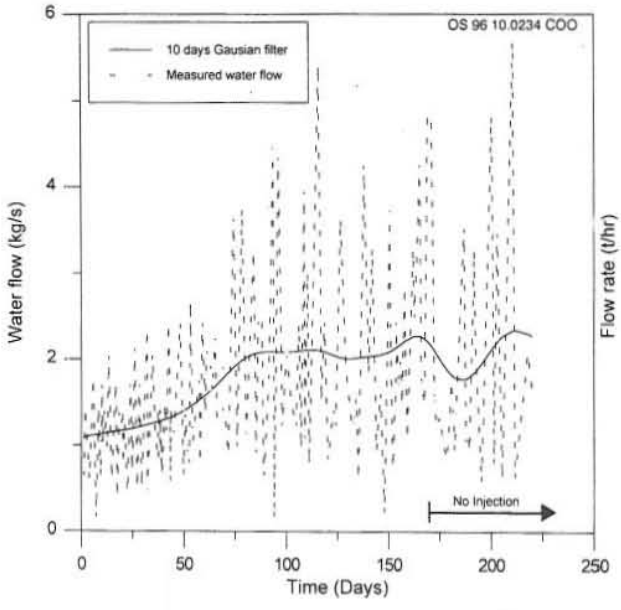

FIGURE 16: Water flow from OW-02 during and after the injection experiment

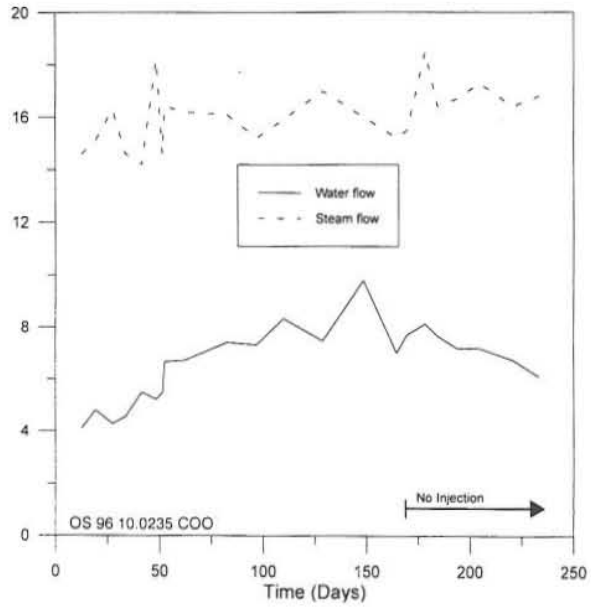

FIGURE 17: Average output from OW-02 during and after the injection experiment

In contrast to well OW-02, well OW-04 was cyclical before the injection experiment but produced at a relatively constant rate during the test. The cyclical nature of the well must therefore, be associated with a deep feed zone which, during the injection, provided a steady flow of low enthalpy water into the well.

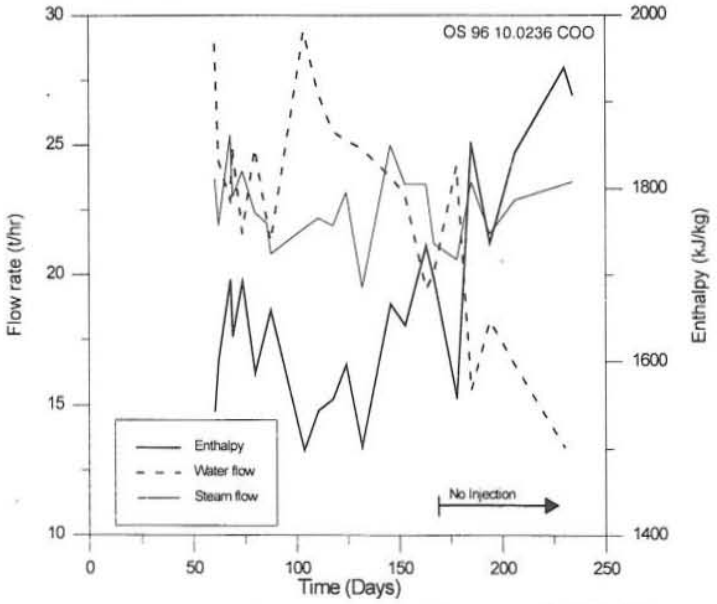

FIGURE 18: Average output from well OW-04 during and after the injection

Figure 19 shows the water flow from well OW-11 during and after injection. This well is 438 m from well OW-03 to the south. It is observed that there is almost no response during the first several days of injection, then a steady increase in water flow rate followed by a near 50 days interval of stabilisation. The water flow then drops suddenly when the injection is stopped. This might also indicate a fracture-like connection to well OW-03 as is the case with well OW-04.

Apart from the three wells mentioned above, no other wells showed changes in output due to injection. One could have expected that well OW-05 which is only 374 m from well OW-03 would have shown some response. It did not, maybe due to its shallow depth (Ambusso, 1994).

Finally, Figure 20 shows some temperature surveys collected in the injection well OW-03 before, during and after injection. It is evident from this figure that all the injected fluid enters the formation at depths greater than 850 m. It should be noticed that the temperature increase in the depth interval 500-800 m during injection is due to inflow of steam rich fluid. This heats up the injection water from 18°C to 40°C. The temperature profile measured before the injection started shows a maximum temperature in the well as 262°C at about 1200 m depth.

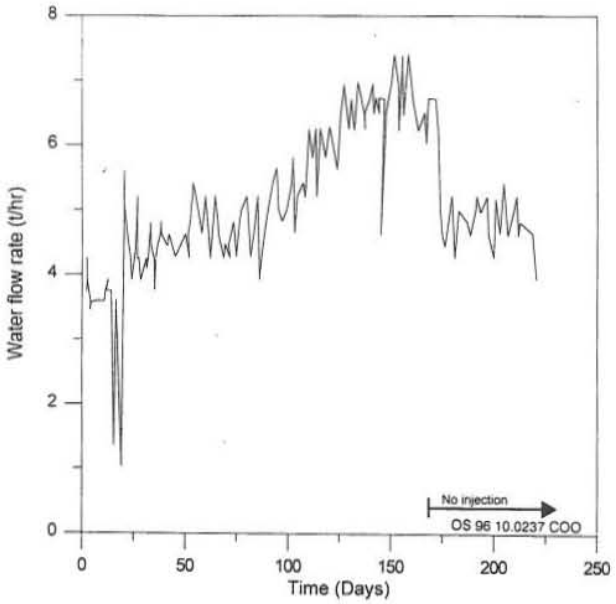

FIGURE 19: Daily water flow from OW-11 during and after injection

By referring to the conceptual model in Figure 11, one may conclude that only the lower, liquid-dominated, section of this reservoir was affected by the injection experiment, at least in the nearest vicinity of injection well OW-03. This conclusion is also supported by steady steam flow but transient water flow in the neighbouring production wells during the test.

5.3 Selecting a model view point for tracer analysis

The tracer data discussed here reflect the nature of different flow paths that connect the injection and production wells. Each of these flow paths represents a sub-volume of the reservoir. Accounting for all the flow paths in the same model is not easy and may not be necessary as the thermal effects of all the flow paths can simply be estimated by superposition.

In this work, therefore, the author decided to treat each flow channel connecting the injection to production wells individually. This means that we are only concerned with the tracer concentration in the reservoir, $C_r(t)$, and the outlet temperature of the fracture that is connecting the two wells (Figure 15).

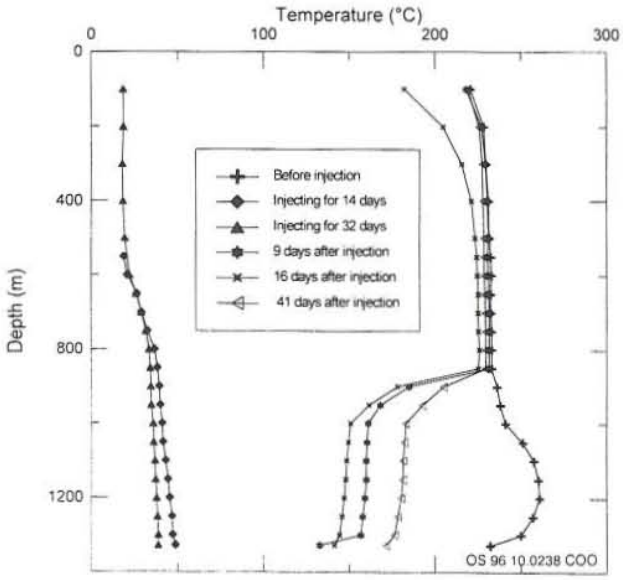

FIGURE 20: Temperature profiles in well OW-03 before, during and after injection

5.4 Converting surface measurements to reservoir values

In order to make use of the 1-D fracture model approach to analyse data from this injection experiment, it is imperative that all measurements done at the surface are converted to flow channel values. This is because the model assumes that all the injected fluid is transported to the production well through fractures connecting the two, carrying the tracer along in them. Tracer concentration at the production well is considered to be that at the fracture outlet.

Conversion of the surface injection flow to fracture flow connecting the injector-producer well dipole is done by multiplying the total surface injection flow by the percentage mass recovery of tracer in this well dipole. The argument here is that if Y % of the total injected tracer is recovered from a certain production well, then the same proportion of the injected water must be flowing to this well. The remaining (100-Y) % flows to other channels in different directions.

The tracer concentration as calculated from the weir box samples is not the same as that at the fracture outlet (entry into the producer well), partly because there could be other feed zones in the producer well contributing more fluid. Also only a fraction of the injected water ends up in the weir box, the rest flows as steam at the separator. The tracer, however, stays in the water phase. If C_r is the tracer concentration at the fracture outlet, q is the flow rate in the fracture, C_w is the tracer concentration in the weir box and m is the weir box water flow, then by conservation of mass

$$C_r = (C_w m)/q \qquad (7)$$

5.5 Tracer recovery analysis

Figure 21 shows the tracer return profile for well OW-04. This curve shows the tracer concentrations in fluid sampled from the weir box and was used to determine the total mass of tracer recovered from this well. A computer program TRMASS (Arason and Björnsson, 1994) was used to calculate the mass

recovered to infinite time. In total, 47.5 kg or 38% of the injected tracer was recovered. From the argument in Section 5.4, it then follows that 47.5 kg of the injected tracer flows via the OW-03 – OW-04 dipole and therefore 10.6 kg/s (38%) of the 28 kg/s injected water flows to well OW-04.

The average weir box flow from well OW-04 during the injection experiment was 7 kg/s and as explained in Section 5.4, the concentration of tracer in the fracture outlet in well OW-04 equals the concentration of tracer at the weir box multiplied by 0.66 (7/10.6). This implies that the tracer recovery curve at the fracture outlet is identical to that at the weir box except that it is scaled down by a factor of 0.66. This is the recovery curve which is used in the model calculations to determine the geometric properties of the fractures connecting these two wells.

Figure 22 shows the inferred and simulated tracer recovery curves for the OW-03 – OW-04 well dipole. The tracer return curves were analysed using the iterative computer program TRINV (Arason and Björnsson, 1994). Due to the high scattering of the measured and hence the inferred data, the model could only match the data with a 53.2% determination. Table 4 presents the model parameters used in the simulation. An average reservoir temperature of 270°C was used in the calculations.

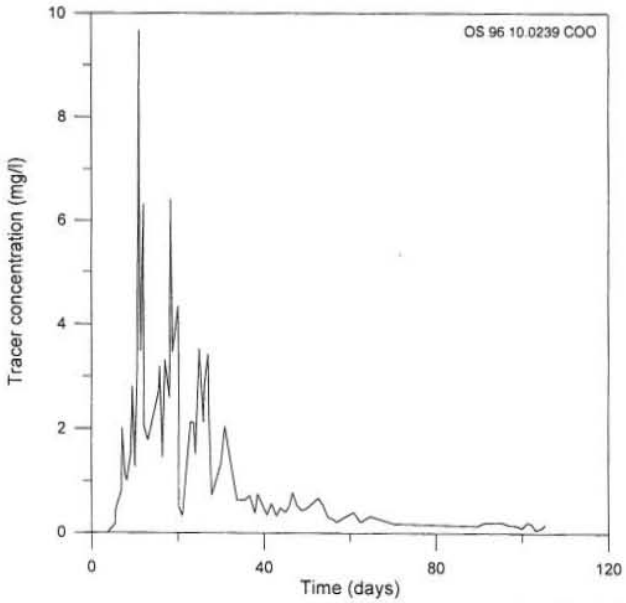

FIGURE 21: Tracer return profile for well OW-04

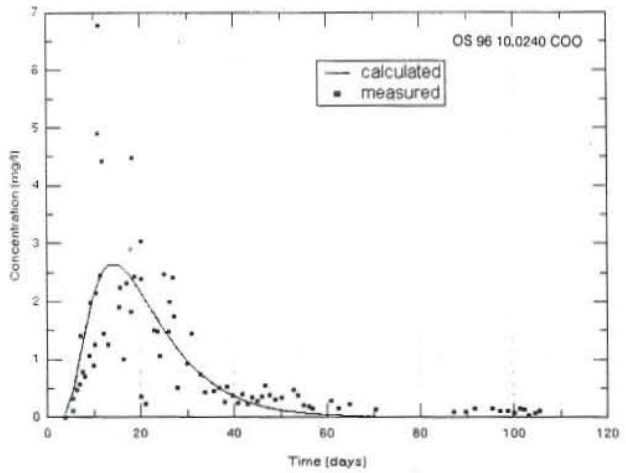

FIGURE 22: Measured and calculated tracer recovery curves for well dipole OW-03 – OW-04

These fracture properties obtained from the tracer studies are finally used in the next section to estimate the heat absorbed by the injected fluid in the fracture system. The assumption is made that the fluid passes through a fracture zone of width 1 m and porosity 50% (Freeze and Cherry, 1979, assigned 5-50% porosity for fractured basalts). This gives a flow height of 210.4 m.

TABLE 4: Model parameters for the OW-03 – OW-04 well dipole

Channel length, x (m)	185
Mean velocity of flow, u (m/hr)	0.47
Dispersion coefficient, D (m^2/s)	0.35×10^{-2}
Combined mass parameter, m (kg/m^2)	0.23
Cross-sectional area of fracture, $A\phi$ (m^2)	105.2
Dispersivity, αL (m)	26.5

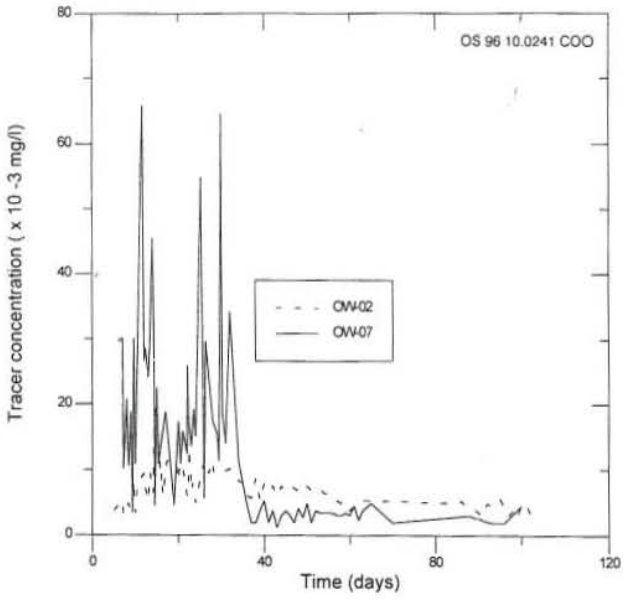

FIGURE 23: Tracer return curves for wells OW-02 and OW-07

Tracer return profiles for OW-02 and OW-07 are shown in Figure 23. These data were very scattered and were complicated further by the fact that the wells are cyclical. The percentage mass recovery of tracer from these wells (0.1% for OW-02 and 0.07% for OW-07) are very low. This may suggest that the tracer underwent thermal degradation, the tracer was adsorbed by the rock matrix between the wells and OW-03, or that only a minor fraction of the injected water flowed towards these wells.

Almost no tracer was detected in OW-11 despite the fact that this well had a considerable increase in water flow during injection and an immediate response after injection implying a direct connection with well OW-03 (Figure 19). This could be explained by the fact that the tracer was totally degraded by the high reservoir temperatures and the long distance (438 m) on its way from well OW-03 to OW-11.

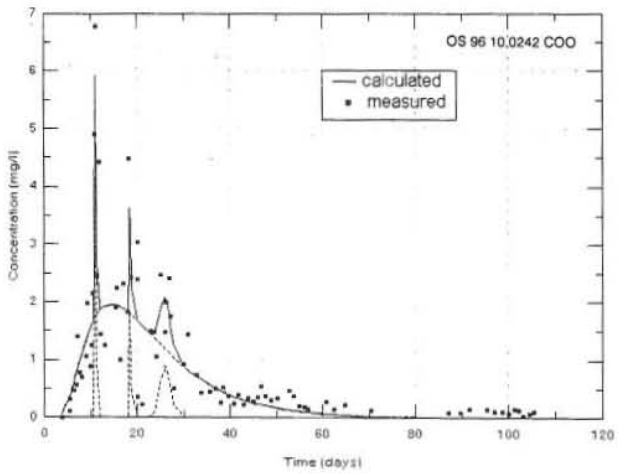

FIGURE 24: Four pulse simulation of tracer recovery in well OW-04

5.6 Sensitivity of the fracture model

The model used in the previous section assumes that only one flow path connects the production-injection wells. The spikes observed in the measured tracer data are considered, in this case, as noise. However, another approach would be to view these spikes as representing tracer breakthroughs for different flow paths between the production-injection wells. Figure 24 shows the results of matching four pulses to the measured tracer data. It shows that the first tracer breakthrough was obtained after 11 days, the second and the most dominant one was obtained after 14 days, the third one was obtained after 18.5 days and the forth was obtained after 25.5 days. The model parameters for this simulation are shown in Table 5.

From Table 5 it is observed that out of the 38% tracer recovered, 90% is contributed by the second pulse and that the cross-sectional area of the fracture (110 m^2) is comparable to 105.2 m^2 obtained in the previous section. It is, therefore, obvious that this model of flow is identical to the single pulse model as a negligible amount of the injected fluid is flowing along the "spike" flow paths.

TABLE 5: Four pulse model parameters for the OW-03 → OW-04 well dipole

Parameter	Pulse 1	Pulse 2	Pulse 3	Pulse 4
Mean velocity of flow, u (m/hr)	0.72	0.47	0.40	0.30
Dispersion coefficient, D (m^2/s)	0.33×10^{-5}	0.40×10^{-2}	0.27×10^{-4}	0.14×10^{-4}
Combined mass parameter, m (kg/m^2)	0.03	0.50	0.02	0.02
Cross-sectional area of fracture, $A\phi$ (m^2)	72	110	119	167
Dispersivity, αL (m)	0.17×10^{-1}	31	0.2×10^{-2}	0.17
Mass recovery %, M_r	2	90	4	4

6. THERMAL PERFORMANCE OF INJECTION-PRODUCTION DIPOLES

6.1 Predictions via the 1-D fracture model

As injection schemes may become an integral part of the management of high-temperature geothermal resources, one must define their positive and negative aspects. As an example, injection may result in pressure recovery in the reservoir but also in enthalpy reduction. These two phenomena may counteract so that the benefits of higher reservoir pressure (additional well output) are overwhelmed by decreasing steam productivity (reduced well output).

The fracture model described in Chapter 4.3 applies here for estimating the thermal performance of an injection-production dipole. The approach is as follows:

1. The analysis of tracer recovery data (Table 4) provides an estimate for the thickness, length and height of a fracture connecting the injection-production wells.
2. Given the range of these geometrical properties, one can use Equation 5 in Chapter 4 to predict the temperature of the injected fluid as it enters the production well (fracture outlet temperature).
3. The calculated outlet temperature of the fractures possibly connecting the injection-production wells is finally used to evaluate the thermal performance of the dipoles.

In the approach by Björnsson et al. (1994), the injection dipole was, for example, only considered to be an operational success if it provided a fracture outlet temperature higher than the return temperature of houses heated by the same geothermal water. Similarly, one can consider fracture outlet temperatures higher than the two-phase separator temperatures to be a minimum requirement for long term injection of "cold" fluids in a productive high-temperature well field.

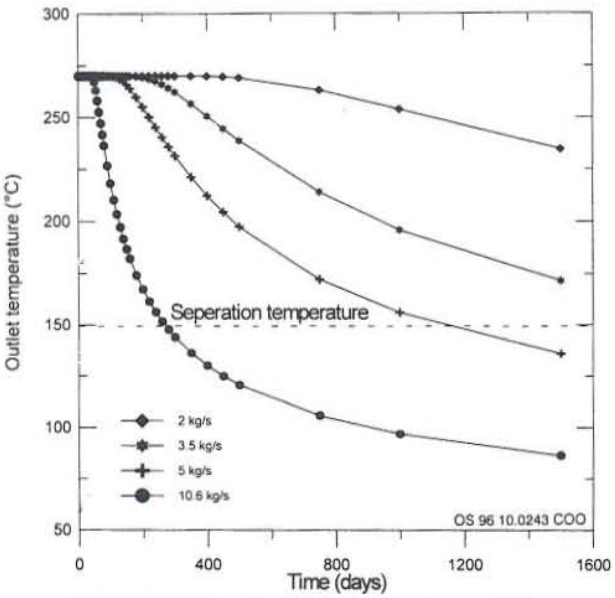

FIGURE 25: Outlet temperature of the OW-03 → OW-04 well dipole for variable injection of 40°C water

Figures 25, 26, and 27 show calculated fracture outlet temperatures of water produced from the well dipole OW-03 → OW-04. Injection of 40°C

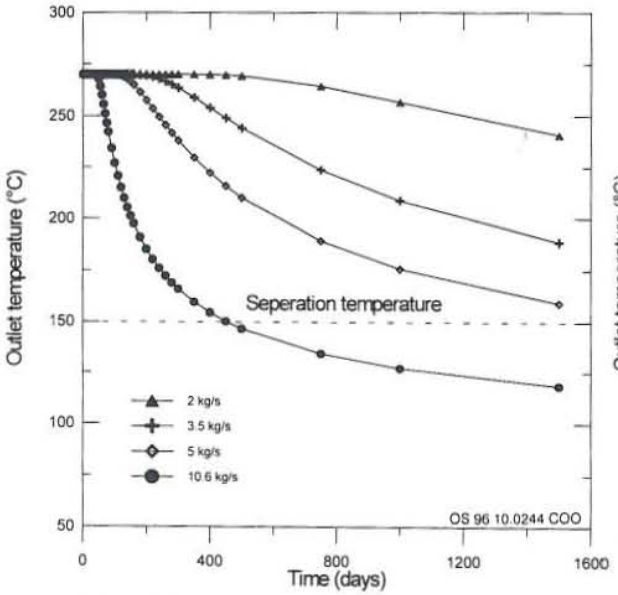

FIGURE 26: Outlet temperature of the OW-03 → OW-04 well dipole if 80°C injection water is used

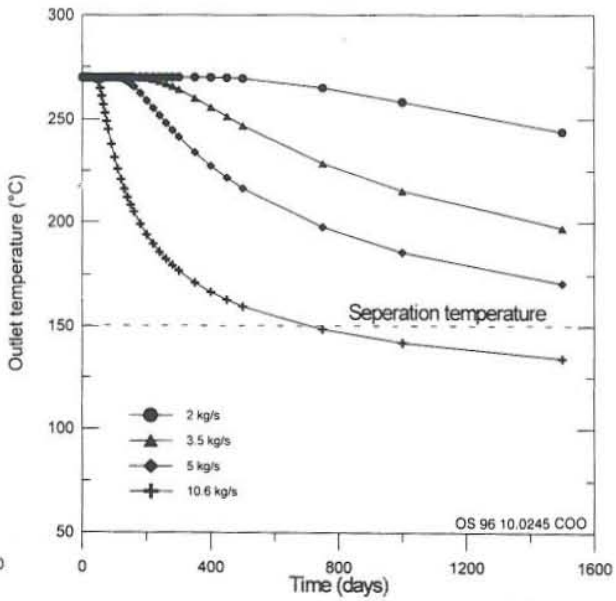

FIGURE 27: Outlet temperature of the OW-03 → OW-04 well dipole if 100°C injection water is used

(18°C at wellhead), 80°C and 100°C water is considered, respectively. The figures show the results for 2, 3.5, 5 and 10.6 kg/s constant injection for a period of 1500 days. A computer program TRCOOL (Arason and Björnsson, 1994) was used to perform these calculations.

To determine the benefits of injection in this sector of Olkaria-East field, a calculation of additional high pressure steam resulting from injection was carried out using a reference pressure, P_s, of 5 bars abs (separator pressure). The mass fraction of steam, X, in the saturated fluid coming from the fracture and separated at 5 bars-a, is then given by the following equation:

$$X = \frac{h_t - h_l(P_s)}{h_s(P_s) - h_l(P_s)} = \frac{4.2T_{out} - 640}{2108} \quad (8)$$

where h_t is the total enthalpy at the fracture outlet (4.2 T_{out}), T_{out} is the fracture outlet temperature and h_l and h_s are the enthalpies of liquid and steam at the separator pressure respectively. The flow rate of additional high pressure steam is then given by X times the injection rate.

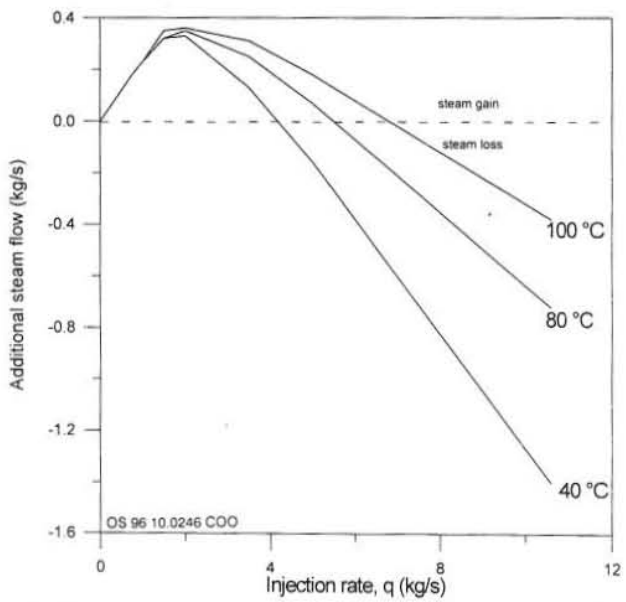

FIGURE 28: Additional high pressure steam after 1500 days injection of 40, 80 and 100°C water into OW-03

Figure 28 shows the additional high pressure steam based on the calculated water temperature at the fracture outlet after 1500 days of injecting 40°C, 80°C and 100°C water. It is observed that injecting 18°C (at wellhead) water for 1500 days can only give additional steam if the injection rate is kept below 4.3 kg/s. However, if the temperature of the

injected water is increased to 100°C, then any injection rate below 7 kg/s will give additional steam.

Figure 29 shows the cumulative steam output from the fracture connecting OW-03 and OW-04 over 1500 days of injection. From this it can be concluded that injection at high flow rates (28 kg/s) in this part of the field is not beneficial due to reservoir cooling even if 100°C water is injected.

Figure 30 finally shows the calculated fracture outlet temperature at a point 438 m away from the injection well as a result of injecting 40°C water into well OW-03. This location corresponds to well OW-11 and the calculation of these temperatures has been based on the fracture properties obtained in the previous section. The assumption here is that the same fracture connects wells OW-03, OW-04 and OW-11. Compared to Figure 25, this figure demonstrates that injection of cold water at high flow rates in this part of the field will have reduced cooling effects if the injection well is located further away from the production wells.

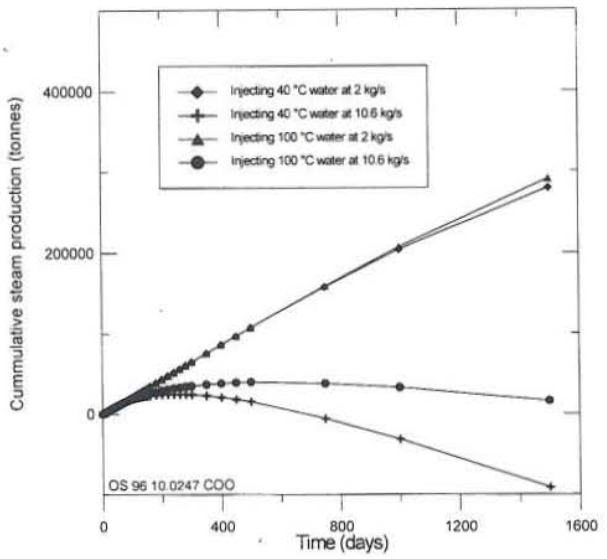

FIGURE 29: Cumulative steam output from OW-03 → OW-04 dipole at different scenarios

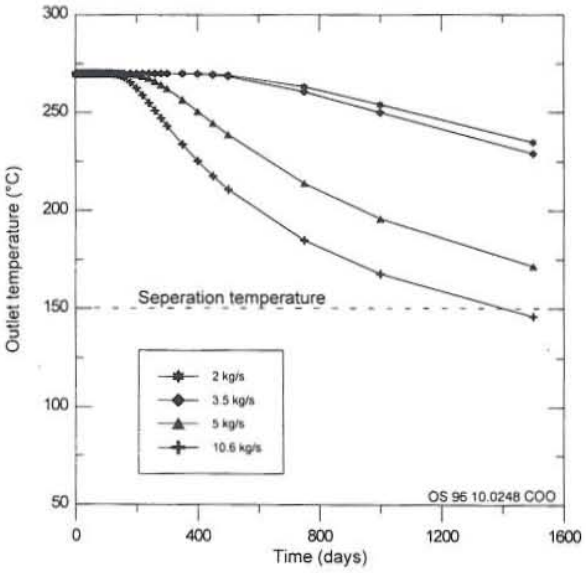

FIGURE 30: Calculated cooling of water at a point 438 m away from OW-03 due to injection of 40°C water (18°C at wellhead)

6.2 Correlation of fracture outlet temperatures to production data

The production data presented in Figures 16-19 show that noticeable changes occur in total enthalpy and weir box flow rates in some of the wells, although the steam flow rates remain relatively constant. It is of interest to correlate these enthalpy and flow rate changes to the calculated fracture outlet temperatures shown in the previous section. Assuming that the injected fluid is only an addition to the well flow rate before injection, the governing equations of mass and heat flow before and during the injection can then be written as:

$$\textit{Enthalpy}: \quad h_2 = (1-\eta)h_1 + \eta h_{fracture} = (1-\eta)h_1 + \eta C_w T_{out} \tag{9}$$

$$\textit{Massflow}: \quad m_2 = m_1 + \Delta m = \Delta m + (1-\eta)m_2 \tag{10}$$

where h is the total enthalpy, C_w is the heat capacity of water, T_{out} is fracture outlet temperature, m is total mass flow rate, Δm *is* the increase in flow due to injection, η is the mass fraction of the injected water in the total flow and subscripts 1 and 2 denote values before and during injection respectively.

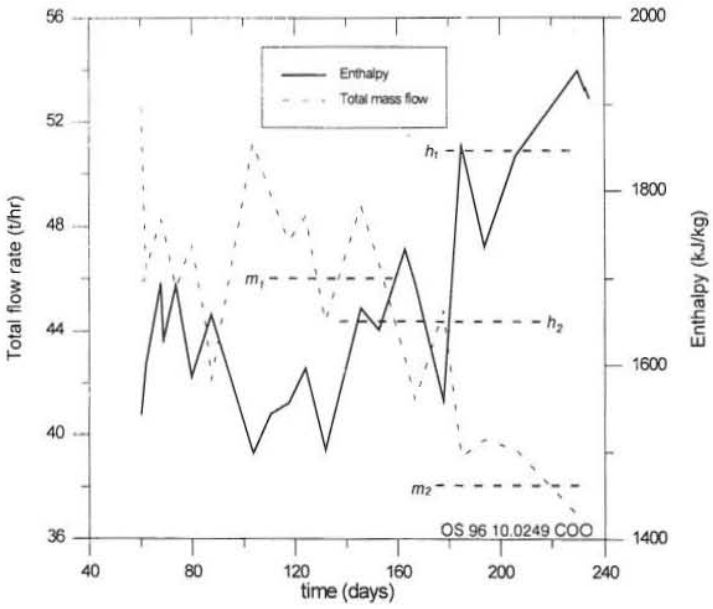

FIGURE 31: Estimation of total flow and enthalpy from OW-04 during and after injection in OW-03

The two equations above are solved simultaneously for η and T_{out}. Figure 31 shows how the values of h_1, h_2, m_1, m_2 (and hence Δm) are estimated from the production data and in this case h_1 =1850 kJ/kg, h_2=1650 kJ/kg, m_1 =38 t/hr and m_2=46 t/hr for well OW-04. Inserting into the two equations above and solving for T_{out} gives a value of 160°C. From Figure 25, the fracture outlet temperature after 170 days injection of 40°C water is approximately 180°C. These two temperature values are thus comparable. However, if the average values of m_1 and h_1 are chosen to be those found during initial well discharge tests, that is 32 t/hr and 1800 kJ/kg (see Table 3), then the fracture outlet temperature becomes 310°C. This is not realistic.

We can, therefore, conclude that the calculated fracture outlet temperatures from the 1-D model may not correlate with the values obtained from the measured production data. The reason is that the changes in weir flow may not necessarily be due to thermal breakthrough of the injected water. It could also be due to increased reservoir pressure around the production wells during injection, hence inhibiting boiling around these wells and making them discharge more water than usual.

7. DISCUSSION

The results of the tracer test show that over 38% of the tracer injected into well OW-03 migrated southwards, at least this amount was recovered in well OW-04 and 0.1% in OW-02. Little tracer was recovered from well OW-02 because, as will be seen below, the connection between this well and OW-03 is possibly matrix dominated so more tracer is absorbed and thermally degraded. Almost no tracer was recovered in well OW-11 due to thermal degradation as a result of the long distance from well OW-03. Very little tracer (0.07%) was recovered from well OW-07 possibly due to either thermal degradation or higher pressures in the north.

The immediate response of water output from wells OW-04 and OW-11 when the injection is stopped compared to that of OW-02, also suggests a fractur-like connection between OW-03 and OW-04/OW-11 and a matrix dominant connection between OW-03 and OW-02. The injected water seems to affect only the water output from the production wells and not the steam output. The reason is that water is transported in the deeper and liquid-dominated part of the reservoir.

Several fractures may actually connect wells OW-03 and OW-04 and this may account for the spikes and early breakthrough time observed in the tracer data. The main flow channel between these two wells is, however, the one with 14 days tracer breakthrough time. A thermal performance analysis was not performed on the basis of this model. It would, however, give more positive results than the single connection model, as the total fracture-fluid contact area would be larger.

8. CONCLUSIONS AND RECOMMENDATIONS

Based on the analysis of the available data and the foregoing discussions, the following conclusions and recommendations can be made:

1. Fluid migration within this reservoir is from north to south and a possible N-S striking fracture exists in the vicinity of wells OW-26, OW-18, OW-15 and OW-16.
2. Siting a production well at a location between OW-18 and OW-26 should be considered.
3. Wells OW-03, OW-04 and OW-11 are connected by a fracture.
4. The injected water travels mainly in the deep liquid-dominated part of the reservoir.
5. Cold water injection in this part of the field is not beneficial and if it has to be done it should be at low injection rates of less than 50 m^3/hr.
6. Hot water injection is more favourable but low injection rates should also be preferred.
7. Injection into a producing field is generally not a good strategy considering the cooling effect in the reservoir and it would be best to site the injection well outside the field and far from the production wells.
8. The sodium fluorescine tracer was thermally degraded and was not recovered from wells located at long distances (>400 m) away from well OW-03.
9. A tracer test involving a radioactive tracer or any other stable non reactive tracer should be tried.
10. The geochemists should review their sampling methods and also the way the tracer is injected.

It is my feeling that the scattering observed in tracer data is more of human origin than due to cycling of wells or multiple return paths. By way of comparison, the tracer return for the potassium iodide tracer test done in Olkaria-NE shows even worse scattering and the several peaks can really not be attributed to multiple return paths or even thermal breakdown (Karingithi, 1995), suggesting that the tracer was not really injected as a slug pulse.

I would also suggest a radioactive tracer be considered for future experiments. This is backed by the fact that tracer tests done in the Ahuachapan geothermal field in El Salvador using I^{131} and I^{125} gave very consistent breakthrough curves (Montalvo, 1996).

ACKNOWLEDGEMENTS

I am greatly indebted to my supervisor, Mr. Grímur Björnsson, for his guidance and support. He dedicated his time and strength to see that this work succeeded. I am also grateful to Mr. Willis Ambusso who despite being far away in the USA, made available for me the data I used in this work. Special thanks go to the UNU and the Government of Iceland for funding this course and to Dr. Ingvar B. Fridleifsson and Mr. Lúdvík S. Georgsson for their good organisation of this course, and to the other lecturers and entire staff of Orkustofnun. I would also thank Mr. Benedikt Steingrímsson, in particular, for critically reading the report. Finally I would like to thank KPLC for granting me a sabbatical leave in order to attend the six months course.

REFERENCES

Ambusso, W.J., 1994: Results of injection and tracer tests in Olkaria-East geothermal field. *Proceedings of the 19th Workshop on Geothermal Reservoir Engineering, Stanford University, California*, 155-160.

Arason, P., and Björnsson, G., 1994: *ICEBOX.*. 2nd edition, Orkustofnun, Reykjavik, 38 pp.

Björnsson, G., Axelsson, G., and Flóvenz, Ó.G., 1994: Feasibility study for the Thelamörk low-temperature system in N-Iceland. *Proceedings of the 19th Workshop on Geothermal Reservoir Engineering, Stanford University, California,* 5-13.

Bödvarsson, G., 1969: On the temperature of water flowing through fractures. *J. Geophys. Res., 74-8,* 1987-1992.

Carslaw, H.W., and Jaeger, J.C., 1959: *Conduction of heat in solids*. 2nd Edition, Claredon Press, Oxford, 510 pp.

Freeze, R.A., and Cherry, J.A., 1979: *Groundwater*. Prentice-Hall Inc., Englewood Cliffs, New Jersey, 604 pp.

Javandel, I., Doughty, C., and Tsang, C.F., 1984: *Groundwater transport: Handbook of mathematical models*. American Geophysical Union, Water Resources Monograph Series 10, 228 pp.

Karingithi, C.W., 1995: *Olkaria-Northeast potassium iodide tracer and injection tests*. The Kenya Power Company Ltd., report.

Kenya Power Company, 1984: *Scientific and technical review meeting report, November 1984.* The Kenya Power Company Ltd., report.

Merz & McLellan-Virkir, 1981: *Recommendations for further geothermal exploration at Olkaria.* The Kenya Power Company Ltd., report.

Merz & McLellan-Virkir, 1985: *Status report on steam production*. The Kenya Power Company Ltd., Olkaria Geothermal Project, internal report.

Merz & McLellan-Virkir, 1986: *Status report on steam production*. The Kenya Power Company Ltd., Olkaria Geothermal Project, internal report.

Montalvo, F.E., 1996: Tracer modelling and heat mining calculations for the Ahuachapan Geothermal Field El Salvador C.A. Report 2 in: *Geothermal Training in Iceland 1996.* UNU G.T.P., Iceland, 1-22.

Naylor, W.I., 1972: *Geology of the Eburru and Olkaria prospects.* U.N. Geothermal Exploration Project, report.

Odongo, M.E.O., 1993: A geological review of Olkaria geothermal reservoir based on structure. *Proceedings of the 15th New Zealand Geothermal Workshop, Geothermal Institute, Auckland,* 169-173.